Journal of Sound and Vibration (2001) **247**(2), 227–242
doi:10.1006/jsvi.2001.3707, available online at http://www.idealibrary.com on IDEAL®

ANALYSIS OF ELASTIC FLEXURAL WAVES IN NON-UNIFORM BEAMS BASED ON MEASUREMENT OF STRAINS AND ACCELERATIONS

L. Hillström and B. Lundberg

The Ångström Laboratory, Uppsala University, Box 534, *SE*-751 21 *Uppsala, Sweden.*
E-mail: *bengt.lundberg@angstrom.uu.se*

(*Received* 17 *December* 1999, *and in final form* 15 *February* 2001)

Elastic flexural waves in an unloaded and unsupported segment of a non-uniform beam were considered. A method based on Timoshenko's model was established for evaluation of shear force, transverse velocity, bending moment and angular velocity at an arbitrary section from four independent measurements of such quantities at one to four sections. From these quantities, shear stress, normal stress, power transmission, etc., can be obtained. Experimental tests were carried out with an aluminium beam which had an abrupt change in height from 15 to 20 mm and was equipped with strain gauges and accelerometers at four uniformly distributed measurement sections and at three evaluation sections. The distance between the two outermost measurement sections was 600 mm, corresponding to 1·12 wavelengths at the upper end of the frequency interval 2–500 Hz considered. Bending moments and transverse velocities evaluated agreed well with those measured at evaluation sections located centrally among the measurement sections and at a distance of 100 mm, or 0·16 wavelengths, outside. At a distance of 500 mm, or 0·82 wavelengths, outside the measurement sections, there was a relatively large disagreement related to a high condition number of a matrix.

1. INTRODUCTION

Generation of elastic flexural waves in beams occurs in different technological processes, often as an unwanted side effect. In percussive drilling of rock, e.g., us e is made of elastic extensional waves, but due to eccentric impacts, imperfect drill rods [1], unsymmetrical loading of the drill bit [2], etc., flexural waves are also generated. This gives rise to leakage of energy from the extensional to the flexural waves, increased stress levels, and increased generation of noise. If the predominant wavelengths are at least of the order of the transverse dimensions of the beam, the motion of flexural waves can be examined by using the Timoshenko beam model. If they are much longer, the wave motion can also be studied by using the Euler–Bernoulli beam model [3].

In various applications, it is interesting to know the histories of shear force, transverse velocity, bending moment and angular velocity associated with flexural waves at one or several sections of a beam. From them, histories of other important quantities such as shear stress, deflection, normal stress, rotation of a cross-section and power transmission can also be determined.

For elastic extensional waves, Lundberg and Henchoz [4] showed that histories of normal force and particle velocity at an arbitrary section of a uniform bar can be evaluated from measured strains at two different sections and by solving time-domain difference equations which are exact in relation to the one-dimensional theory used. A similar method

0022-460X/01/420227 + 16 $35.00/0

was used by Yanagihara [5] to determine impact force. Lagerkvist and Lundberg [6], Lagerkvist and Sundin [7] and Sundin [8] used the method to determine mechanical point impedance. The method was also used by Karlsson *et al.* [9] in a study of the interaction of rock and bit in percussive drilling. It was extended to non-uniform bars by Lundberg *et al.* [10], and this version of the method was used for determination of force–displacement relationships for different combinations of drill bits and rocks by Carlsson *et al.* [11] and for high-temperature fracture mechanics testing by Bacon *et al.* [12, 13]. The use of the method was extended to visco-elastic extensional waves by Bacon [14, 15], and to elastic flexural waves by Sundin and Åhrström [16] who assessed frictional properties and lubricant performance at an obliquely impacted end of a long uniform beam from acceleration measurements at two sections.

The aim of the present paper is to develop a general method for evaluation of the histories of shear force, transverse velocity, bending moment and angular velocity at a section E of a non-uniform beam from measurements of such quantities at different sections A, B, C and D. It will be shown that, for an unloaded segment of the beam, this can be achieved through measurement of four such quantities which differ from each other in terms of either section (A, B, C and D) or type of quantity (shear force, transverse velocity, bending moment and angular velocity), or both.

First, the method will be developed on the basis of Timoshenko's beam model. Then, experimental impact tests with a non-uniform beam made of aluminium and equipped with strain gauges and accelerometers will be presented, and comparisons will be made between (i) bending moments and particle velocities evaluated at section E on the basis of measurements at sections A–D and (ii) the same quantities measured at section E.

2. THEORETICAL BASIS

2.1. FORMULATION OF THE PROBLEM

Consider a segment of a non-uniform Timoshenko beam with the cross-sectional area $A(x)$, moment of inertia $I(x)$, Young's modulus $E(x)$, shear modulus $G(x)$ and density $\rho(x)$, where x is a co-ordinate along the straight centreline of the beam. For a rectangular cross-section, as in the experimental part, $A = WH$ and $I = WH^3/12$, where W is the width and H is the height. The shear modulus is related to Young's modulus through $G = E/2(1 + \nu)$, where ν is the Poisson ratio. Within the beam segment, there must be no loads, supports, joints or spots of contact. Outside, where there are no such restrictions, the beam is assumed to interact with supports, structures and loads. The supports and structures may have linear or non-linear responses, and they are assumed to have the capability to absorb energy associated with vibrations. Furthermore, the loads are assumed to act during finite time. Otherwise, nothing needs to be known about supports, structures or loads outside the beam segment under consideration.

The beam is quiescent for time $t < 0$, and for $t \geqslant 0$ it is subjected to a transverse load with finite duration. As a consequence, there will be a deflection of centreline $w(x,t)$ and a rotation of cross-section $\phi(x, t)$. In the beam segment considered, these deflections and rotations are governed by the equations of motion

$$\frac{\partial Q}{\partial x} = \rho A \frac{\partial^2 w}{\partial t^2}, \qquad -Q + \frac{\partial M}{\partial x} = \rho I \frac{\partial^2 \phi}{\partial t^2}, \tag{1}$$

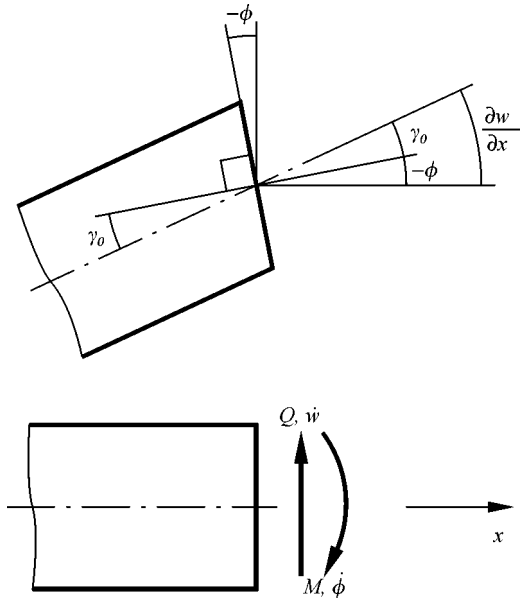

Figure 1. Angles ϕ, γ_0, $\partial w/\partial x$, shear force Q, transverse velocity $\dot{w}$, bending moment M and angular velocity $\dot{\phi}$ at a general section x of the beam.

respectively, where $Q(x, t)$ is the transverse shear force and $M(x, t)$ is the bending moment. The deflections and rotations are related to each other through

$$\frac{\partial w}{\partial x} = -\phi + \gamma_0, \tag{2}$$

where γ_0 is the shear strain on the centreline as shown in Figure 1. The terms $-\phi$ and γ_0 on the right-hand side represent the contributions to the slope of the centreline of the beam from bending and shear, respectively, and they are related to the bending moment and the transverse shear force through

$$M = EI\frac{\partial \phi}{\partial x}, \qquad Q = \kappa GA\gamma_0, \tag{3}$$

where κ is a dimensionless quantity which depends on the shear stress distribution and therefore on the shape of the cross-section. According to beam theory, this quantity can be determined from the relation $\kappa = [(A/I^2)\int (S^2/W^2)\,\mathrm{d}A]^{-1}$, where the static moment S and in general also the width W depend on the vertical co-ordinate z from the centreline. For a rectangular cross-section, this formula gives $\kappa = 5/6 \approx 0{\cdot}83$, which is the value to be used in the experimental part. According to another definition, κ may depend also on the Poisson ratio.

Equations (1)–(3) provide five relations between the five unknown functions $Q(x, t)$, $w(x, t)$, $M(x, t)$, $\phi(x, t)$ and $\gamma_0(x, t)$. Through elimination of $\gamma_0(x, t)$, these relations can be transformed into the system of four first order partial differential equations

$$\frac{\partial Q}{\partial x} = \rho \mathrm{A}\frac{\partial \dot{w}}{\partial t}, \quad \frac{\partial \dot{w}}{\partial x} = \frac{1}{\kappa GA}\frac{\partial Q}{\partial t} - \dot{\phi}, \quad \frac{\partial M}{\partial x} = Q + \rho I\frac{\partial \dot{\phi}}{\partial t}, \quad \frac{\partial \dot{\phi}}{\partial x} = \frac{1}{EI}\frac{\partial M}{\partial t} \tag{4}$$

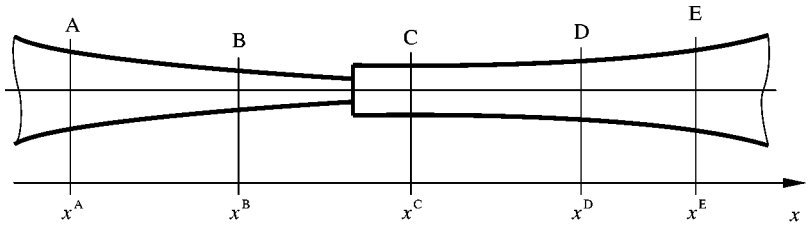

Figure 2. Unloaded section of non-uniform beam in the general case. Sections of measurement A–D and of evaluation E.

for the four quantities $Q(x, t)$, $\dot{w}(x, t) = \partial w(x, t)/\partial t$, $M(x, t)$ and $\dot{\phi}(x, t) = \partial \phi(x, t)/\partial t$. These quantities constitute the elements of a state vector $\mathbf{s}(x, t) = [Q, \dot{w}, M, \dot{\phi}]^T$, which is zero for $t < 0$. Furthermore, because of energy absorption outside the beam segment considered, $\mathbf{s}(x, t) \to \mathbf{0}$ as $t \to \infty$.

The problem to be solved is as follows. Consider the four elements Q, $\dot{w}$, M and $\dot{\phi}$ of the state vector $\mathbf{s}$ at four different sections A, B, C and D of the beam segment, i.e., altogether 16 elements. Let four out of them, constituting the elements of a vector $\mathbf{m}$, be known from measurements for $t \geqslant 0$. Then, determine the state vector $\mathbf{s}$ or its Fourier transform $\hat{\mathbf{s}}$ (which is assumed to exist) at any section E of the beam segment. See Figure 2, where it is indicated that the variation of the geometrical and material properties along the beam segment may be continuous or discontinuous.

2.2. SOLUTION IN THE GENERAL CASE

Fourier transformation of relations (4) gives

$$\hat{\mathbf{s}}' = \mathbf{R}\hat{\mathbf{s}}, \tag{5}$$

where

$$\mathbf{R} = \begin{bmatrix} 0 & i\omega\rho A & 0 & 0 \\ i\omega/\kappa GA & 0 & 0 & -1 \\ 1 & 0 & 0 & i\omega\rho I \\ 0 & 0 & i\omega/EI & 0 \end{bmatrix} \tag{6}$$

is the system matrix,

$$\hat{\mathbf{s}} = \begin{bmatrix} \hat{Q} \\ \hat{\dot{w}} \\ \hat{M} \\ \hat{\dot{\phi}} \end{bmatrix} \tag{7}$$

is the Fourier transform of the state vector $\mathbf{s}$, i.e., $\hat{\mathbf{s}}(x, \omega) = \int_{-\infty}^{\infty} \mathbf{s}(x, t) e^{-i\omega t} dt$, and $\hat{\mathbf{s}}' = \partial \hat{\mathbf{s}}/\partial x$.

The state at any section x is related to that at the fixed section x^0 through

$$\hat{\mathbf{s}}(x, \omega) = \mathbf{P}(x, x^0, \omega)\hat{\mathbf{s}}(x^0, \omega). \tag{8}$$

Here, by equations (5) and (8), the transition matrix $\mathbf{P}(x, x^0, \omega)$ satisfies

$$\mathbf{P}' = \mathbf{RP}, \quad \mathbf{P}(x^0, x^0, \omega) = \mathbf{I}, \tag{9}$$

where $\mathbf{I}$ is the identity matrix. In particular, equation (8), with $x^0 = x^{\mathrm{E}}$ and with $x = x^{\mathrm{A}}$, x^{B}, x^{C} and x^{D}, gives

$$\mathbf{P}^{\mathrm{AE}}\hat{\mathbf{s}}^{\mathrm{E}} = \hat{\mathbf{s}}^{\mathrm{A}}, \quad \mathbf{P}^{\mathrm{BE}}\hat{\mathbf{s}}^{\mathrm{E}} = \hat{\mathbf{s}}^{\mathrm{B}}, \quad \mathbf{P}^{\mathrm{CE}}\hat{\mathbf{s}}^{\mathrm{E}} = \hat{\mathbf{s}}^{\mathrm{C}}, \quad \mathbf{P}^{\mathrm{DE}}\hat{\mathbf{s}}^{\mathrm{E}} = \hat{\mathbf{s}}^{\mathrm{D}} \tag{10}$$

for the segments AE, BE, CE and DE.

The problem of determining the state vector $\hat{\mathbf{s}}^{\mathrm{E}}$ from the knowledge of four out of the 16 elements of the state vectors $\hat{\mathbf{s}}^{\mathrm{A}}$, $\hat{\mathbf{s}}^{\mathrm{B}}$, $\hat{\mathbf{s}}^{\mathrm{C}}$ and $\hat{\mathbf{s}}^{\mathrm{D}}$ can now be solved as follows. Four scalar equations, with linear combinations of the elements of $\hat{\mathbf{s}}^{\mathrm{E}}$ in their left-hand members and the measured elements of $\hat{\mathbf{s}}^{\mathrm{A}}$, $\hat{\mathbf{s}}^{\mathrm{B}}$, $\hat{\mathbf{s}}^{\mathrm{C}}$ and $\hat{\mathbf{s}}^{\mathrm{D}}$ in their right-hand members, are singled out from the 16 scalar equations represented by equations (10). They form a system of four linear equations for the four elements of $\hat{\mathbf{s}}^{\mathrm{E}}$ which can, at least in principle, be solved uniquely if the determinant of this system is different from zero. It should be noted that the order of sections A–E along the beam is arbitrary, that section E may coincide with any one of sections A–D, and also that all sections A–D need not be involved in the measurements.

As a first illustration, consider the measurement of the bending moment M at each section A–D. In this case, the third scalar equation from each of the matrix equations (10) give the system

$$\begin{bmatrix} P_{31}^{\mathrm{AE}} & P_{32}^{\mathrm{AE}} & P_{33}^{\mathrm{AE}} & P_{34}^{\mathrm{AE}} \\ P_{31}^{\mathrm{BE}} & P_{32}^{\mathrm{BE}} & P_{33}^{\mathrm{BE}} & P_{34}^{\mathrm{BE}} \\ P_{31}^{\mathrm{CE}} & P_{32}^{\mathrm{CE}} & P_{33}^{\mathrm{CE}} & P_{34}^{\mathrm{CE}} \\ P_{31}^{\mathrm{DE}} & P_{32}^{\mathrm{DE}} & P_{33}^{\mathrm{DE}} & P_{34}^{\mathrm{DE}} \end{bmatrix} \begin{bmatrix} \hat{Q}^{\mathrm{E}} \\ \hat{w}^{\mathrm{E}} \\ \hat{M}^{\mathrm{E}} \\ \hat{\phi}^{\mathrm{E}} \end{bmatrix} = \begin{bmatrix} \hat{M}^{\mathrm{A}} \\ \hat{M}^{\mathrm{B}} \\ \hat{M}^{\mathrm{C}} \\ \hat{M}^{\mathrm{D}} \end{bmatrix}, \tag{11}$$

which can also be written as

$$\begin{bmatrix} P_{31}^{\mathrm{AE}} & P_{32}^{\mathrm{AE}} & P_{33}^{\mathrm{AE}} & P_{34}^{\mathrm{AE}} \\ P_{31}^{\mathrm{BE}} & P_{32}^{\mathrm{BE}} & P_{33}^{\mathrm{BE}} & P_{34}^{\mathrm{BE}} \\ P_{31}^{\mathrm{CE}} & P_{32}^{\mathrm{CE}} & P_{33}^{\mathrm{CE}} & P_{34}^{\mathrm{CE}} \\ P_{31}^{\mathrm{DE}} & P_{32}^{\mathrm{DE}} & P_{33}^{\mathrm{DE}} & P_{34}^{\mathrm{DE}} \end{bmatrix} \begin{bmatrix} \hat{s}_1^{\mathrm{E}} \\ \hat{s}_2^{\mathrm{E}} \\ \hat{s}_3^{\mathrm{E}} \\ \hat{s}_4^{\mathrm{E}} \end{bmatrix} = \begin{bmatrix} \hat{s}_3^{\mathrm{A}} \\ \hat{s}_3^{\mathrm{B}} \\ \hat{s}_3^{\mathrm{C}} \\ \hat{s}_3^{\mathrm{D}} \end{bmatrix}. \tag{12}$$

As a second illustration, consider the measurement of the transverse velocity $\dot{w}$ at each of sections A–D. In this case, the second scalar equation from each of the matrix equations (10) give the system

$$\begin{bmatrix} P_{21}^{\mathrm{AE}} & P_{22}^{\mathrm{AE}} & P_{23}^{\mathrm{AE}} & P_{24}^{\mathrm{AE}} \\ P_{21}^{\mathrm{BE}} & P_{22}^{\mathrm{BE}} & P_{23}^{\mathrm{BE}} & P_{24}^{\mathrm{BE}} \\ P_{21}^{\mathrm{CE}} & P_{22}^{\mathrm{CE}} & P_{23}^{\mathrm{CE}} & P_{24}^{\mathrm{CE}} \\ P_{21}^{\mathrm{DE}} & P_{22}^{\mathrm{DE}} & P_{23}^{\mathrm{DE}} & P_{24}^{\mathrm{DE}} \end{bmatrix} \begin{bmatrix} \hat{Q}^{\mathrm{E}} \\ \hat{\dot{w}}^{\mathrm{E}} \\ \hat{M}^{\mathrm{E}} \\ \hat{\phi}^{\mathrm{E}} \end{bmatrix} = \begin{bmatrix} \hat{\dot{w}}^{\mathrm{A}} \\ \hat{\dot{w}}^{\mathrm{B}} \\ \hat{\dot{w}}^{\mathrm{C}} \\ \hat{\dot{w}}^{\mathrm{D}} \end{bmatrix}, \tag{13}$$

which can also be written as

$$\begin{bmatrix} P_{21}^{AE} & P_{22}^{AE} & P_{23}^{AE} & P_{24}^{AE} \\ P_{21}^{BE} & P_{22}^{BE} & P_{23}^{BE} & P_{24}^{BE} \\ P_{21}^{CE} & P_{22}^{CE} & P_{23}^{CE} & P_{24}^{CE} \\ P_{21}^{DE} & P_{22}^{DE} & P_{23}^{DE} & P_{24}^{DE} \end{bmatrix} \begin{bmatrix} \hat{s}_1^E \\ \hat{s}_2^E \\ \hat{s}_3^E \\ \hat{s}_4^E \end{bmatrix} = \begin{bmatrix} \hat{s}_2^A \\ \hat{s}_2^B \\ \hat{s}_2^C \\ \hat{s}_2^D \end{bmatrix}. \tag{14}$$

In the general case, equations (12) and (14) take the form

$$\begin{bmatrix} P_{e_1 1}^{c_1 E} & P_{e_1 2}^{c_1 E} & P_{e_1 3}^{c_1 E} & P_{e_1 4}^{c_1 E} \\ P_{e_2 1}^{c_2 E} & P_{e_2 2}^{c_2 E} & P_{e_2 3}^{c_2 E} & P_{e_2 4}^{c_2 E} \\ P_{e_3 1}^{c_3 E} & P_{e_3 2}^{c_3 E} & P_{e_3 3}^{c_3 E} & P_{e_3 4}^{c_3 E} \\ P_{e_4 1}^{c_4 E} & P_{e_4 2}^{c_4 E} & P_{e_4 3}^{c_4 E} & P_{e_4 4}^{c_4 E} \end{bmatrix} \begin{bmatrix} \hat{s}_1^E \\ \hat{s}_2^E \\ \hat{s}_3^E \\ \hat{s}_4^E \end{bmatrix} = \begin{bmatrix} \hat{s}_{e_1}^{c_1} \\ \hat{s}_{e_2}^{c_2} \\ \hat{s}_{e_3}^{c_3} \\ \hat{s}_{e_4}^{c_4} \end{bmatrix} \tag{15}$$

or

$$\mathbf{M}\hat{\mathbf{s}}^E = \hat{\mathbf{m}}, \tag{16}$$

where

$$M_{jk} = P_{e_j k}^{c_j E}, \quad \hat{m}_j = \hat{s}_{e_j}^{c_j}. \tag{17}$$

Here, $\mathbf{M}$ is a matrix with elements M_{jk} singled out from the elements of the transition matrices $\mathbf{P}^{AE}$, $\mathbf{P}^{BE}$, $\mathbf{P}^{CE}$ and $\mathbf{P}^{DE}$, and $\hat{\mathbf{m}}$ is a vector with elements $\hat{m}_j$ of measured quantities at different sections of the beam (j and $k = 1, 2, 3$ or 4). The subscript $e_j = 1, 2, 3$ or 4 defines the type of quantity ($\hat{Q}$, $\hat{w}$, $\hat{M}$ or $\hat{\phi}$, respectively) and the superscript $c_j = \mathrm{A}, \mathrm{B}, \mathrm{C}$ or D, the section associated with $\hat{m}_j$. These quantities define the measurements.

Equation (16) gives the state vector

$$\hat{\mathbf{s}}^E = \mathbf{M}^{-1}\hat{\mathbf{m}}, \tag{18}$$

in terms of the matrix $\mathbf{M}$ and the vector $\hat{\mathbf{m}}$ of measured quantities. Transformation into the time domain gives the state vector $\mathbf{s}^E(t)$ for $t \geqslant 0$. This solves the problem.

2.3. BEAM WITH PIECEWISE CONSTANT PROPERTIES

If the beam has piecewise constant properties as indicated in Figure 3, the transition matrices in equations (10) can be expressed as the products $\mathbf{P}^{AE} = \mathbf{P}^s\mathbf{P}^{s-1}\ldots\mathbf{P}^1, \ldots,$

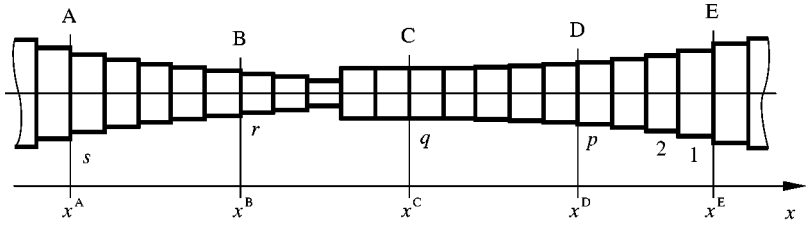

Figure 3. Unloaded section of beam with piece-wise constant properties. Sections of measurement A–D and of evaluation E.

$\mathbf{P}^{\mathrm{DE}} = \mathbf{P}^{p}\mathbf{P}^{p-1} \ldots \mathbf{P}^{1}$, respectively, of transition matrices $\mathbf{P}^{1}, \mathbf{P}^{2}, \ldots, \mathbf{P}^{s}$ for beam elements with constant properties. These matrices, in turn, can be determined by first solving problem (9) for matrices $\mathbf{R}$ which are independent of x, and then substituting appropriate values for x and x^0. This procedure can be simplified by replacing the coupled problem (9) for the elements of $\mathbf{P}$ with an uncoupled problem as follows.

For $\mathbf{R}$ independent of x, equation (9a) gives

$$\mathbf{P}' = \mathbf{RP}, \quad \mathbf{P}'' = \mathbf{R}^2\mathbf{P}, \quad \mathbf{P}''' = \mathbf{R}^3\mathbf{P}, \quad \mathbf{P}^{\mathrm{IV}} = \mathbf{R}^4\mathbf{P}. \tag{19}$$

The eigenvalues γ of the matrix $\mathbf{R}$ are given by the four roots of $|\mathbf{R} - \gamma\mathbf{I}| = 0$, i.e., with the use of definition (6),

$$\gamma^4 + 2a\gamma^2 - b = 0, \tag{20}$$

where

$$a = \frac{\rho\omega^2}{2E}\left(1 + \frac{E}{\kappa G}\right), \quad b = \frac{\rho A\omega^2}{EI}\left(1 - \frac{\rho I\omega^2}{\kappa GA}\right). \tag{21}$$

Thus, there are the two pairs of eigenvalues

$$\gamma = \pm\,\alpha, \quad \gamma = \pm\,\mathrm{i}k, \tag{22}$$

where

$$\alpha = [(b + a^2)^{1/2} - a]^{1/2}, \quad k = [(b + a^2)^{1/2} + a]^{1/2} \tag{23}$$

are both real and positive provided that

$$|\omega| < \left(\frac{\kappa GA}{\rho I}\right)^{1/2}, \tag{24}$$

which is presumed. According to the Cayley–Hamilton theorem, equation (20) for the eigenvalues of the matrix $\mathbf{R}$ is also satisfied by $\mathbf{R}$, i.e.,

$$\mathbf{R}^4 + 2a\mathbf{R}^2 - b\mathbf{I} = \mathbf{0}. \tag{25}$$

Multiplication by $\mathbf{P}$ from the right and use of relations (19b, d) gives the fourth order differential equation

$$\mathbf{P}^{\mathrm{IV}} + 2a\mathbf{P}'' - b\mathbf{P} = \mathbf{0}. \tag{26a}$$

Furthermore, relation (9b) and (19a–c) give the conditions

$$\mathbf{P}(x^0, x^0, \omega) = \mathbf{I}, \quad \mathbf{P}'(x^0, x^0, \omega) = \mathbf{R}, \quad \mathbf{P}''(x^0, x^0, \omega) = \mathbf{R}^2, \quad \mathbf{P}'''(x^0, x^0, \omega) = \mathbf{R}^3 \tag{26b–e}$$

for $x = x^0$. Thus, the coupled problem (9) for the elements of $\mathbf{P}$ has been replaced by the uncoupled problem (26), which has the solution

$$\begin{aligned}\mathbf{P}(x, x^0, \omega) = {} & \mathbf{A}\cos[k(x - x^0)] + \mathbf{B}\sin[k(x - x^0)] \\ & + \mathbf{C}\cosh[\alpha(x - x^0)] + \mathbf{D}\sinh[\alpha(x - x^0)]\end{aligned} \tag{27}$$

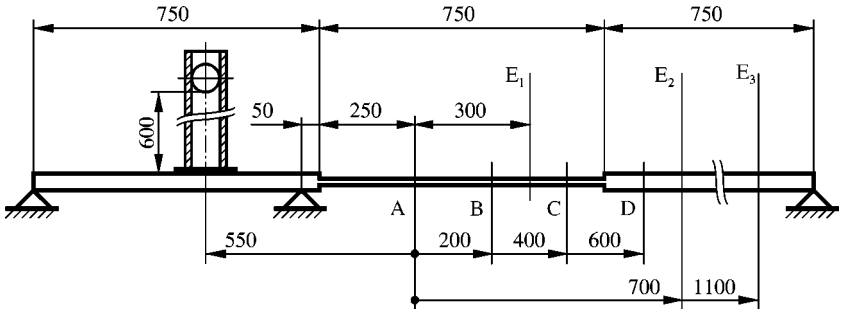

Figure 4. Experimental set-up. Dimensions in mm.

with

$$\mathbf{A} = \frac{1}{\alpha^2 + k^2}(\alpha^2\mathbf{I} - \mathbf{R}^2), \quad \mathbf{B} = \frac{1}{k(\alpha^2 + k^2)}(\alpha^2\mathbf{R} - \mathbf{R}^3),$$

$$\mathbf{C} = \frac{1}{\alpha^2 + k^2}(k^2\mathbf{I} + \mathbf{R}^2), \quad \mathbf{D} = \frac{1}{\alpha(\alpha^2 + k^2)}(k^2\mathbf{R} + \mathbf{R}^3). \tag{28}$$

3. EXPERIMENTAL TESTS

The experimental set-up is illustrated in Figure 4. A beam made of aluminium (AA 6061-T6; $E = 70$ GPa, $\nu = 0{\cdot}3$ and $\rho = 2700\,\mathrm{kg/m^3}$) with rectangular cross-section and length 2250 mm was used. The width W of the beam was 20 mm, while its height H was 15 mm in the central third and 20 mm in the two outer thirds. The beam was held in position by three supports with positions as shown. Each of these supports was realized with a pair of 15 mm wide clamps clad with 1·5 mm thick rubber plates. The beam was impacted laterally by a spherical steel ball which was guided by a tube and dropped from a height of 600 mm. The diameter of the ball was 50 mm, and its mass was 535 g. A 3 mm thick rubber plate at the impacted spot of the beam served to reduce the excitation at high frequencies. The maximum stresses determined from strain measurements on the beam were approximately 30 MPa which is well below the yield stress.

The beam was instrumented with strain gauges and accelerometers at sections A–D and E_1–E_3 as shown in Figure 4. The positions of the strain gauges coincided with these sections, while those of the accelerometers were displaced by 20 mm to the right, i.e., away from the spot of impact. The strain gauges (TML FLA-5-23-1L) were glued (Tokyo Sokki Kenkyujo Co, Ltd, Adhesive CN) to the beam in pairs with one on the top and the other on the bottom. The gauges of each pair were connected to a bridge amplifier (Measurement Group 2210) in opposite branches, so that the output of the amplifier was proportional to the difference between the two strains, and therefore to the bending moment M at the section. Shunt calibration was used. Accelerometers (Brüel & Kjær, three Type 4374 and two Type 4393) were attached with thin layers of wax. The accelerometers were connected to charge amplifiers (three Kistler Type 5011 and two Brüel & Kjær Type 2635).

The amplified strain and accelerometer signals were fed to analogue aliasing filters (DIFA Measuring Systems, PDF) with cut-off frequency 17·5 kHz. The filtered signals were recorded in a time interval $[0, t_{re}]$, with $t_{re} \approx 0{\cdot}25$ s, by two synchronized four-channel digital oscilloscopes (Nicolet Pro 20 and Pro 40) which used a sampling interval of 20 μs. At the end of this time interval, the amplitudes of the recorded signals were reduced to about

TABLE 1

Cases of experimental tests

Case	Input A–D	Output			High-pass filter
		E_1	E_2	E_3	
1	M	M	M	M	No
2	M	$\dot{w}$	$\dot{w}$	$\dot{w}$	No
3	$\dot{w}$	—	$\dot{w}$	—	No
4	$\dot{w}$	—	M	—	Yes

a tenth due to the damping action of the supports. The recorded signals were transferred to a computer for evaluation of the state vector $\mathbf{s}^E(t)$. First, measured accelerations, if any, were integrated to velocities. After use of the FFT algorithm, $\hat{\mathbf{s}}^E(\omega)$ was determined according to equation (18). Finally, $\hat{\mathbf{s}}^E(\omega)$ was transformed into the time domain by use of the inverse FFT algorithm. Results were produced for the same time interval $[0, t_{re}]$ although sometimes they may be valid only in a narrower interval $[0,t_{ev}]$. When, e.g., section E is located outside AD, as in some of the experimental tests, there is a certain difference between t_{re} and t_{ev} which is related to the travel times for flexural waves from section E to sections A–D.

Four test cases, labelled 1–4, are defined in Table 1. In Case 1, bending moments M at sections A–D and E_1–E_3 were determined from measurements of strains at the same sections. In Case 2, bending moments M at sections A–D and transverse velocities $\dot{w}$ at E_1–E_3 were determined from measurements of strains and accelerations, respectively, at the same sections. In Case 3, transverse velocities $\dot{w}$ at sections A–D and E_2 were determined from measurements of accelerations at the same sections. In Case 4, finally, transverse velocities $\dot{w}$ at sections A–D and bending moment M at E_2 were determined from measured accelerations and strains, respectively, at the same sections. In this case, the signals representing accelerations and strains were passed through eight-pole Butterworth high-pass filters with cut-off frequency 10 Hz. In each of the four cases, bending moments M or transverse velocities $\dot{w}$ at sections E_1–E_3, corresponding to the measurements made at these sections, were also determined from those measured at A–D according to equation (18). All tests were carried out at room temperature.

4. RESULTS

Figure 5 shows for Case 1 the condition number cond($\mathbf{M}$) of the matrix $\mathbf{M}$ as a function of the position x^E of section E and of the frequency $f = \omega/2\pi$. It can be seen that the condition number is low, which implies low sensitivity to errors, if section E is inside or not too far outside the segment AD, and if the frequency is neither too low nor too high. Also, it can be noted that the condition number has a peak (limited in height by the step in frequency) near 850 Hz. Similar results were obtained for other cases.

Figure 6 shows results in the time and frequency domains at section E_1 for Case 1. In Figure 6(a), the time-domain results are based on frequencies up to 500 Hz, which means that frequencies around 850 Hz are excluded, while in Figure 6(b) they are based on frequencies up to 2000 Hz. As there is a significantly better agreement between evaluated and measured bending moments in the former case, the results for Cases 1–4 shown in Figures 7–10 are based on frequencies up to 500 Hz.

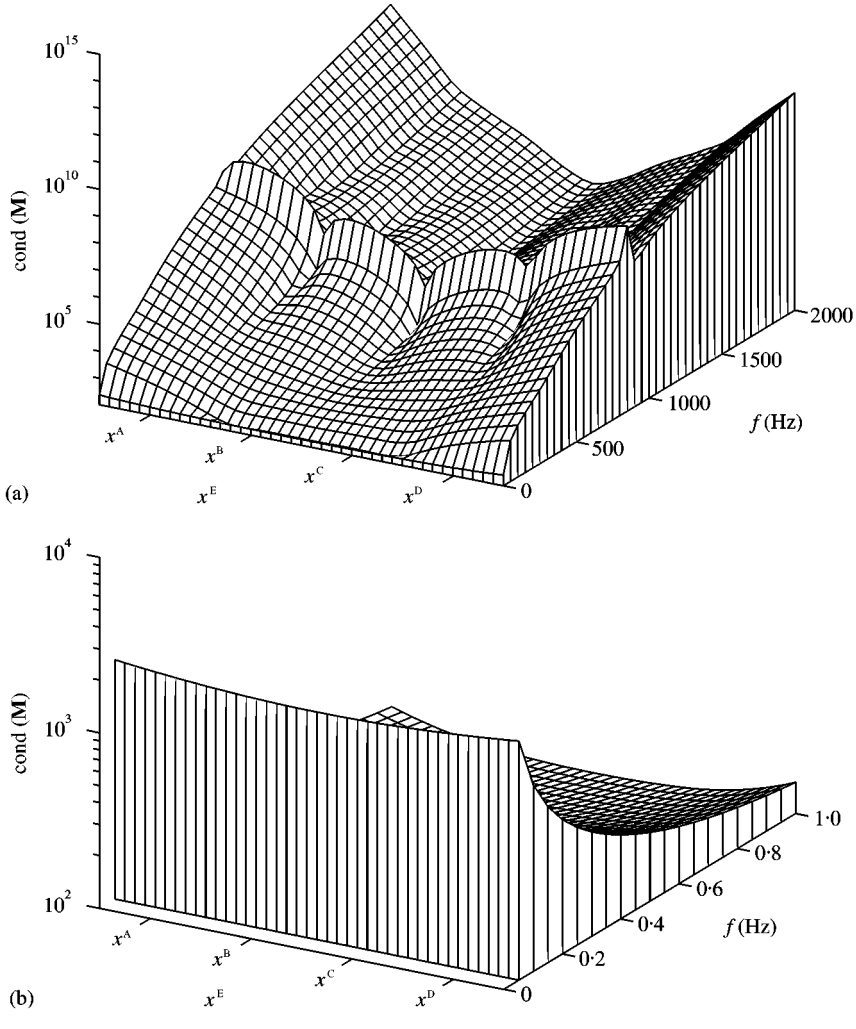

Figure 5. Condition number cond (**M**) of matrix **M** versus position x^E and frequency f in Case 1. (a) 1 Hz $< f <$ 2000 Hz and (b) 0·05 Hz $< f <$ 1 Hz.

5. DISCUSSION

It has been shown how the elements Q, $\dot{w}$, M and $\dot{\phi}$ of the state vector **s** at any section E of an unloaded segment of a non-uniform beam can be determined from independent measurements of four such elements at up to four different sections A, B, C and D of the same unloaded segment of the beam. This has also been demonstrated experimentally. Once the state vector has been determined, several quantities of importance can be obtained from its elements. Thus, e.g., the shear stress τ can be obtained from Q, the normal stress σ from M, the deflection w from $\dot{w}$, and the rotation of the cross-section ϕ from $\dot{\phi}$. Also, the power transmission can be obtained from the relation $P = -(Q\dot{w} + M\dot{\phi})$. Nothing needs to be known about supports, structures and loads outside the beam segment under consideration.

The combination of sections, among A, B, C and D, and types of quantities to be measured, among Q, $\dot{w}$, M and $\dot{\phi}$, can be chosen in many ways, some of which appear to be more convenient than others. Thus, it is straightforward to determine bending moment

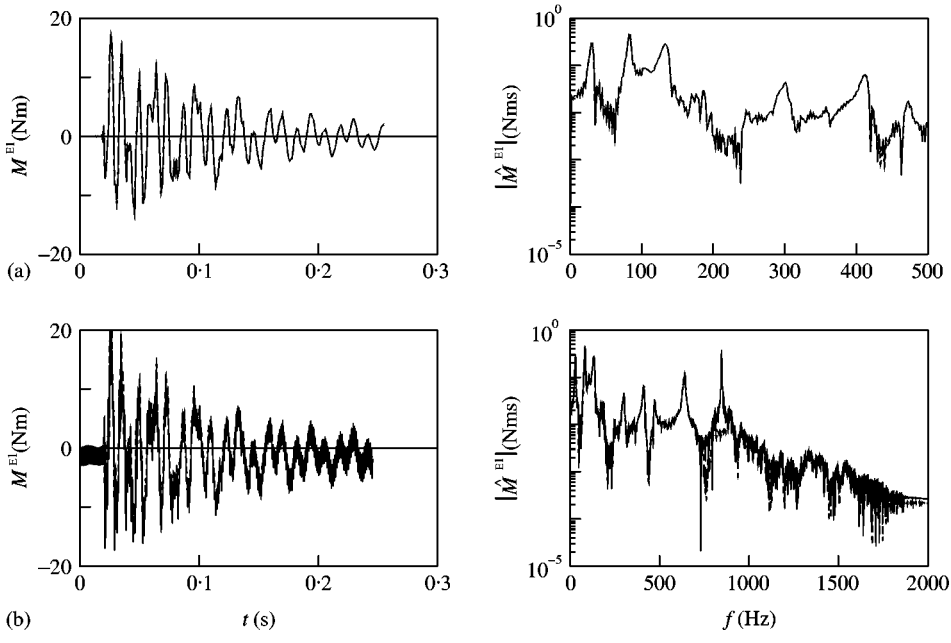

Figure 6. Bending moment M^{E1} versus time t and $|\hat{M}^{E1}|$ versus frequency f. Comparison between bending moment at E_1 evaluated from bending moments measured at A–D (solid curves) and bending moment measured at E_1 (dotted curves) in Case 1. Results for frequencies up to (a) 500 Hz and (b) 2000 Hz.

M from measured strains and transverse velocity $\dot{w}$ from measured accelerations, as was done in the experimental part, while it is less convenient to determine Q or $\dot{\phi}$ from measurements. Also, it seems preferable to place at most two types of transducers at any section A–D of the beam, and to make the same kind of measurement or measurements at each instrumented section. Therefore, two interesting possibilities might be measurement of (i) M at each section A–D (Cases 1 and 2) and (ii) $\dot{w}$ at each section A–D (Cases 3 and 4) as in the experimental part. A third interesting possibility might be the measurement of (iii) both M and $\dot{w}$ at each of two sections, e.g., A and B. It should also be noted that a free end A, with $Q^A \equiv 0$ and $M^A \equiv 0$, can be used to replace two measurements.

The functions $\alpha(\omega)$ and $k(\omega)$ introduced in equations (22) and (23) can be interpreted as follows. Let the state vector have the form $\hat{\mathbf{s}} = \hat{\mathbf{s}}^* \exp(\beta x)$. Then, substitution into equation (5) gives the eigenvalue problem $\mathbf{R}\hat{\mathbf{s}}^* = \beta\hat{\mathbf{s}}^*$. The eigenvalues β are given by the four roots of equation (20) with $\beta = \gamma$. Thus, according to equation (22), the eigenvalues are $\beta = \pm\alpha$ and $\beta = \pm ik$. Therefore, provided that condition (24) is satisfied as presumed, α determines the decay of non-propagating (evanescent) modes and k is the wave number of propagating harmonic waves ($\omega > 0$).

For angular frequencies $|\omega| \ll \omega_0 = c_0/R$, where $c_0 = (E/\rho)^{1/2}$ is the speed of elastic extensional waves and $R = (I/A)^{1/2}$ is the radius of inertia of the cross-section, equations (23) can be approximated by $\alpha \approx k \approx b^{1/4}$ and equation (21b) by $b \approx (\rho A/EI)\omega^2$. As the wave number k is related to the wavelength λ by $k = 2\pi/\lambda$, one obtains $\alpha \approx 2\pi/\lambda$ with $\lambda \approx 2\pi(c_0 R/|\omega|)^{1/2} \gg 2\pi R$. In terms of the frequency $f = \omega/2\pi$ and the height $H = 2\sqrt{3}R$ of a beam with rectangular cross-section, the corresponding relations are $|f| \ll f_0 = c_0/\theta H$, $\alpha \approx 2\pi/\lambda$, and $\lambda \approx (c_0\theta H/|f|)^{1/2} \gg \theta H$, with $\theta = \pi/\sqrt{3}$. These low-frequency approximations of α and λ represent the limiting case of the Euler–Bernoulli beam.

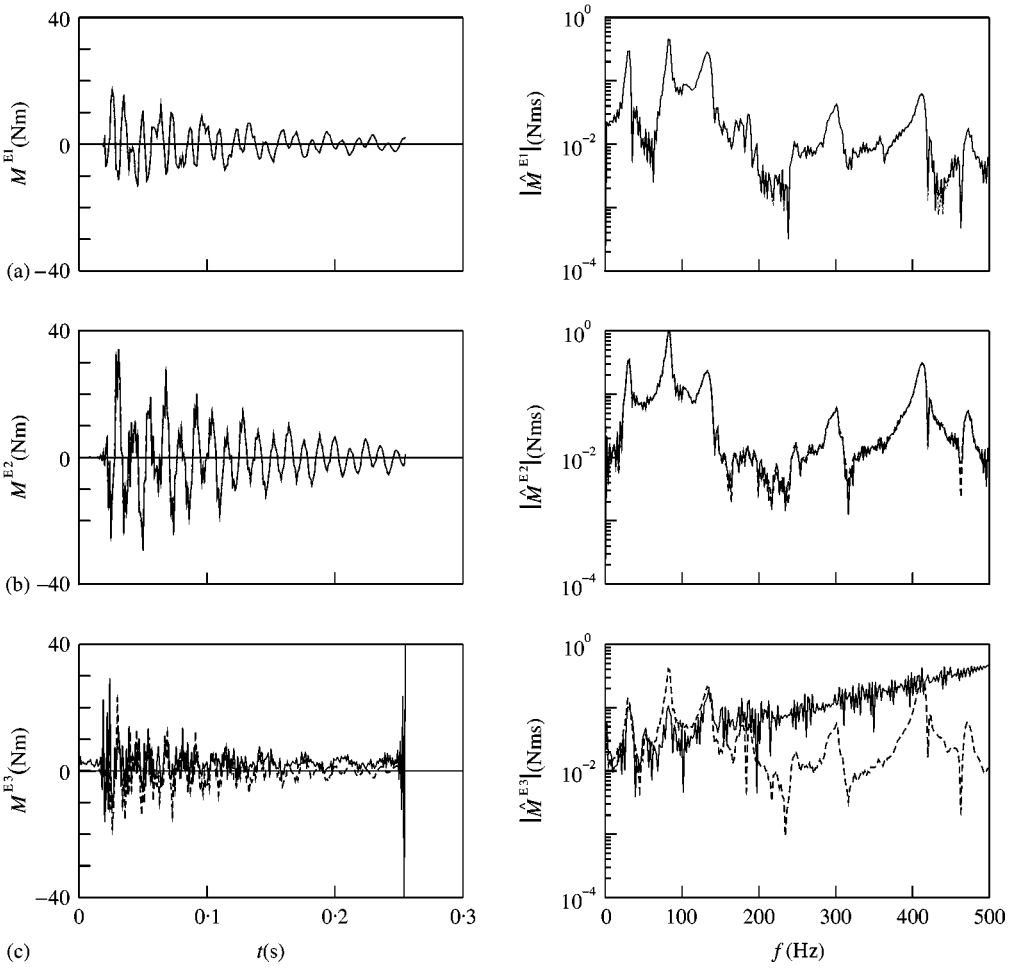

Figure 7. Bending moments (a) M^{E1} versus time t and $|\hat{M}^{E1}|$ versus frequency f, (b) M^{E2} versus time t and $|\hat{M}^{E2}|$ versus frequency f, and (c) M^{E3} versus time t and $|\hat{M}^{E3}|$ versus frequency f. Comparison between bending moments at E_1–E_3 evaluated from bending moments measured at A–D (solid curves) and bending moment measured at E_1–E_3 (dotted curves) in Case 1. Results for frequencies up to 500 Hz.

For the aluminium beam used in the experimental tests, the highest frequency normally considered, 500 Hz, corresponds to the wavelengths 0·606 and 0·525 m in the segments with heights 20 and 15 mm respectively. Similarly, the frequency 2000 Hz, considered in Figure 6, corresponds to the wavelengths 0·300 and 0·260 m, respectively. Thus, in the tests carried out, the wavelengths were much larger than the heights of the beam, and $|f| \ll f_0$. This means that the above approximations are accurate and also that condition (24) is satisfied as it can be written as $|f| < f_0[\kappa/2(1+\nu)]^{1/2}$.

In the time domain, solution (18) corresponds to a deconvolution. When the condition number of the matrix $\mathbf{M}$ is high (cf. Figure 5), the sensitivity of this solution to measurement errors and numerical errors may be high. Such situations are related to the transition matrices $\mathbf{P}^{AE}, \ldots,$ and $\mathbf{P}^{DE}$, which determine the elements of the matrix $\mathbf{M}$. Therefore, it is useful to note from equation (27) that, for a uniform beam and relatively low frequencies with $\alpha \approx 2\pi/\lambda$, these transition matrices contain terms proportional to $e^{2\pi(x^E - x^A)/\lambda}, \ldots,$ and $e^{2\pi(x^E - x^D)/\lambda}$ respectively. In the discussion which follows, it is assumed that $x^A < x^B < x^C < x^D$ and that $x^A < x^E$.

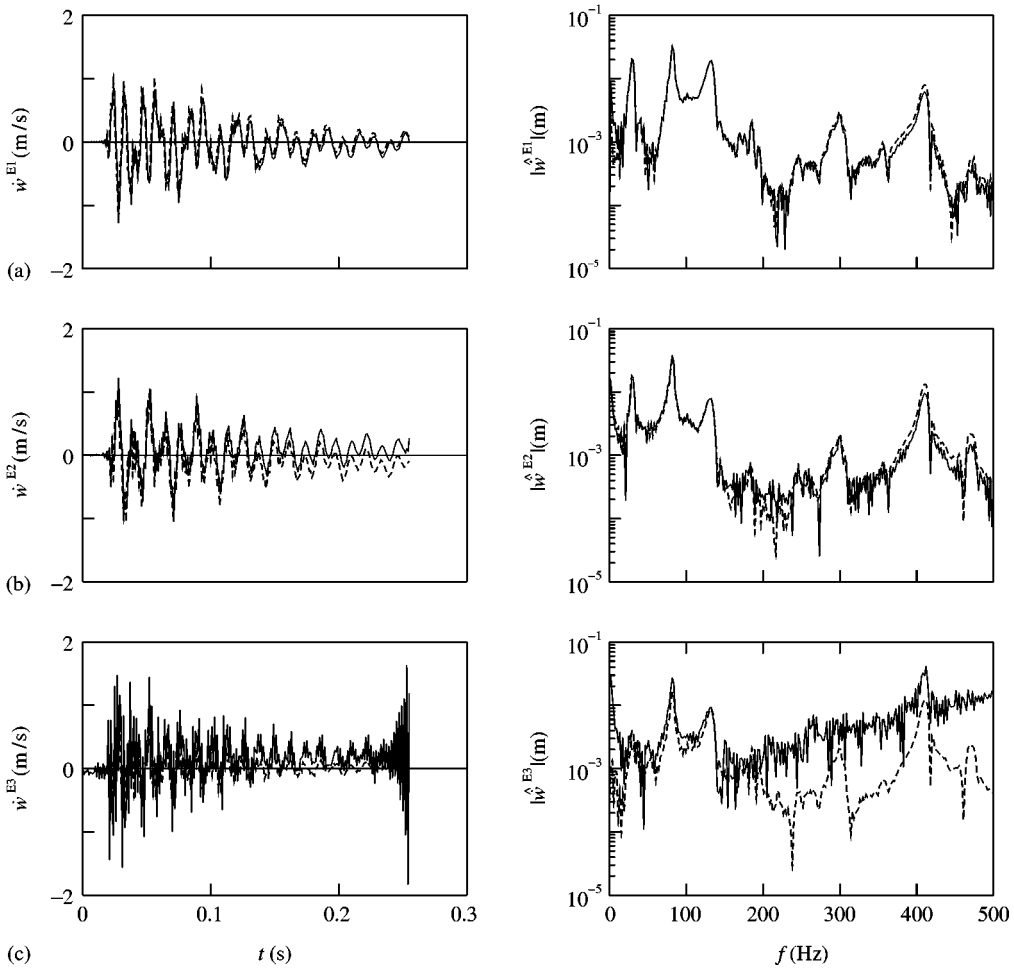

Figure 8. Transverse velocities (a) $\dot{w}^{E1}$ versus time t and $|\hat{\dot{w}}^{E1}|$ versus frequency f, (b) $\dot{w}^{E2}$ versus time t and $|\hat{\dot{w}}^{E2}|$ versus frequency f, and (c) $\dot{w}^{E3}$ versus time t and $|\hat{\dot{w}}^{E3}|$ versus frequency f. Comparison between transverse velocities at E_1–E_3 evaluated from bending moments measured at A–D (solid curves) and transverse velocities measured at E_1–E_3 (dotted curves) in Case 2. Results for frequencies up to 500 Hz.

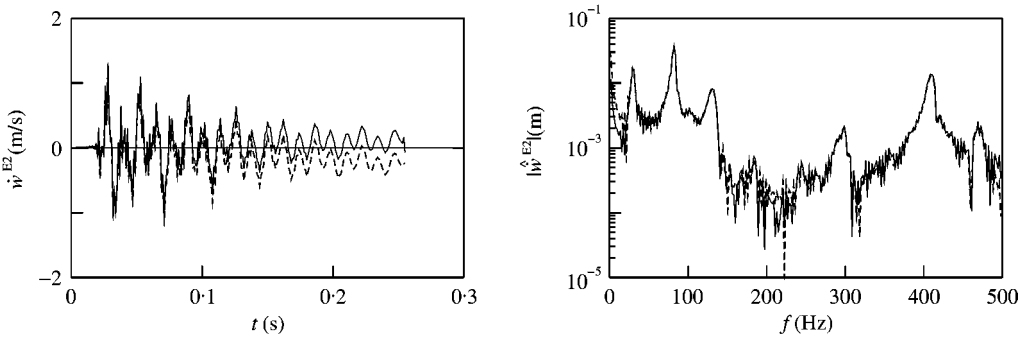

Figure 9. Transverse velocity $\dot{w}^{E2}$ versus time t and $|\hat{\dot{w}}^{E2}|$ versus frequency f. Comparison between transverse velocity at E_2 evaluated from transverse velocities measured at A–D (solid curves) and transverse velocity measured at E_2 (dotted curves) in Case 3. Results for frequencies up to 500 Hz.

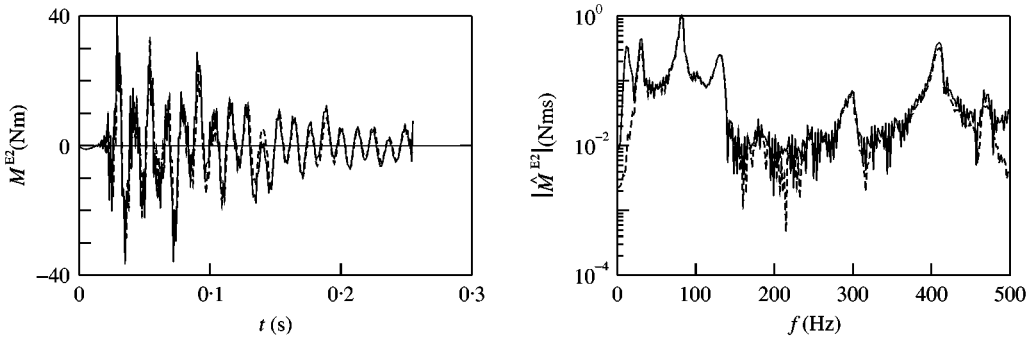

Figure 10. Bending moment M^{E2} versus time t and $|\hat{M}^{E2}|$ versus frequency f. Comparison between bending moment evaluated at E_2 from transverse velocities measured at A–D (solid curves) and bending moment measured at E_2 (dotted curves) in Case 4. Results for frequencies up to 500 Hz.

The matrix **M** may be ill-conditioned at low frequencies corresponding to long wave lengths which make the four scalar equations, represented by equation (11), nearly the same. It may also be ill-conditioned at high frequencies corresponding to short wavelengths which make the magnitudes of the elements in the different rows of the matrix **M** very different. Thus, e.g., the ratio $e^{2\pi(x^D - x^A)/\lambda}$ of the exponential factors of the first row to those of the fourth row of the matrix **M** in equation (11) quickly grows with the ratio $(x^D - x^A)/\lambda$. In the experimental tests, the distance AD (600 mm) was only slightly longer than one wavelength ($\approx 1{\cdot}12\lambda$) at the highest frequency 500 Hz, corresponding to the ratio $e^{2{\cdot}24\pi} \approx 1{\cdot}1 \times 10^3$. The matrix **M** may also be ill-conditioned near discrete frequencies which make distances between adjacent sections A–D equal to an integral multiple of a half wavelength. In Case 1, the distances AB and BC in the thinner central section of the beam are one half wavelength at a frequency of about 860 Hz, which may explain the high sensitivity to errors around 850 Hz illustrated in Figure 5. This problem and those at high frequencies were avoided in the experimental tests by considering only frequencies below 500 Hz. Furthermore, the matrix **M** may be ill-conditioned if section E is far outside the segment AD. This has the effect that the coefficients of the four scalar equations represented by equation (11) become very large. The largest coefficients, containing exponential factors $e^{2\pi(x^E - x^A)/\lambda}$, occur in the first of these equations. In the experimental tests, the distances AE_1, AE_2 and AE_3 were approximately 0·57, 1·28 and 1·94 wavelengths at the highest frequency 500 Hz. Thus, E_1 was located at the centre of the beam segment AD, while E_2 and E_3 were located at distances 0·16 and 0·82 wavelengths, respectively, outside this segment. These locations correspond to the exponential factors $e^{1{\cdot}14\pi} \approx 3{\cdot}6 \times 10^1$, $e^{2{\cdot}56\pi} \approx 3{\cdot}1 \times 10^3$ and $e^{3{\cdot}88\pi} \approx 2{\cdot}0 \times 10^5$ respectively.

The effects of noise may be reduced by use of Wiener filtering techniques [17]. Also, a conceivable way of avoiding integral multiples of half wavelengths between adjacent sections A–D, which might allow frequencies considerably higher than 500 Hz, would be to make use of more than four measurements, so that system (16) for the elements of $\hat{\mathbf{s}}^E$ would be overdetermined, and of a non-uniform distribution of instrumented sections. This way of eliminating critical frequencies has been found to be effective in an application involving viscoelastic extensional waves [18].

For Case 1, Figure 7 shows that there is an excellent agreement in the frequency range 2–500 Hz between (i) the bending moment evaluated at section E_1 from measurements of bending moments at sections A–D and (ii) the bending moment measured at the same section E_1. For section E_2 the agreement is very good in the same range of frequencies. For section E_3 there is relatively large disagreement, in particular at high frequencies

corresponding to short wavelengths and large exponential factors $e^{2\pi(x^E - x^A)/\lambda}$. In the time domain there is particularly large disagreement near $t \approx t_{re} \approx 0{\cdot}25$ s.

For Case 2, Figure 8 shows that there is a good agreement in the frequency range 10–500 Hz between (i) the transverse velocity evaluated at section E_1 from measurements of bending moments at sections A–D and (ii) the transverse velocity measured at the same section E_1. For section E_2, the agreement is fair in the same range of frequencies. For section E_3, there is again relatively large disagreement, in particular at high frequencies corresponding to short wavelengths and large exponential factors $e^{2\pi(x^E - x^A)/\lambda}$, and in the time domain near $t \approx t_{re} \approx 0{\cdot}25$.

Cases 1 and 2 show that the quality of the evaluated results is generally high when section E is located within the segment AD, whereas it rapidly decays outside. This is consistent with the rapid increase of the condition number outside the segment AD shown in Figure 5 for Case 1. The large disagreement near $t \approx t_{re} \approx 0{\cdot}25$ s for section E_3 in both cases is believed to be due to the difference between t_{re} and t_{ev} mentioned in the experimental part. Thus, where the large errors occur, information from section E_3 may not yet have reached sections A–D to the extent required. This error can be avoided by recording signals till all waves are damped out. Then, t_{re} and t_{ev} can be considered to be arbitrarily large.

For Case 3, Figure 9 shows that there is a fair agreement in the frequency range 20–500 Hz between (i) the transverse velocity evaluated at section E_2 from measurements of transverse velocities at sections A–D and (ii) the transverse velocity measured at the same section E_2. For Case 4, Figure 10 shows that there is a fair agreement in the same range of frequencies between (i) the bending moment evaluated at section E_2 from measurements of transverse velocities at sections A–D and (ii) the bending moment measured at the same section E_2.

It should be noted that the accelerometers used are quite inaccurate below 10 Hz. This inaccuracy is reflected by the disagreement between evaluated and measured quantities below 10–20 Hz in Cases 2–4. The fair agreement in Case 4 was obtained by using the Butterworth high-pass filters which reduced this disagreement.

In this paper, use has been made of transition matrices which relate the state vectors (with elements Q, $\dot{w}$, M and $\dot{\phi}$) at the two ends of a beam element. As an alternative, it would be possible to make use of the corresponding dynamic stiffness matrices which relate the generalized forces (Q and M) to the generalized velocities ($\dot{w}$ and $\dot{\phi}$) at the two ends of the same beam element. For the beam segment considered (the structure), this approach would result in a system $\mathbf{Zv} = \mathbf{F}$, where $\mathbf{Z}$ is the dynamic stiffness matrix, $\mathbf{v}$ is the vector of generalized nodal velocities, and $\mathbf{F}$ is the vector of generalized nodal forces. This is the approach of the so-called exact displacement method which was developed by Kolousek [19] in the early 1940s and implemented for plane frame analysis by Åkesson [20]. If the number of nodes of the beam segment considered is to be n, the matrix $\mathbf{Z}$ would be $2n \times 2n$ and the vector $\mathbf{v}$ would contain $2n$ generalized velocities. Also, in addition to zeroes, the vector $\mathbf{F}$ would contain four generalized nodal forces (two at each end node of the beam segment considered). Thus, there would be a system of $2n$ relations between $2n + 4$ generalized velocities and forces. If four of these quantities are measured, then generally the system $\mathbf{Zv} = \mathbf{F}$ can be solved for those which remain. Although the uses of transition matrices and dynamic stiffness matrices are formally equivalent, an advantage of the former approach, which was chosen here, is that the state vector $\hat{\mathbf{s}}^E$, with its four elements, and the vector $\mathbf{m}$, with the measured quantities as its elements, appear explicitly in the system $\mathbf{M}\hat{\mathbf{s}}^E = \hat{\mathbf{m}}$. Another advantage is the connection between the wave phenomena in the beam, the properties of the matrix $\mathbf{M}$, and the accuracy of the results brought about by the functions $\alpha(\omega)$ and $k(\omega)$.

ACKNOWLEDGMENTS

Funding of this research from the Carl Trygger Foundation, the Swedish Council for Engineering Sciences and AB Sandvik Tamrock Tools is gratefully acknowledged.

REFERENCES

1. R. Beccu, C. M. Wu and B. Lundberg 1996 *Journal of Sound and Vibration* **191**, 261–272. Reflection and transmission of the energy of transient elastic extensional waves in a bent bar.
2. I. Carlvik 1981 *International Journal of Rock Mechanics, Mining Science and Geomechanical Abstracts* **10**, 167–172. The generation of bending vibrations in drill rods.
3. K. F. Graff 1975 *Wave motion in elastic solids*. Mineola, New York: Dover Publications, Reprinted edition, 1991.
4. B. Lundberg and A. Henchoz 1977 *Experimental Mechanics* **17**, 213–218. Analysis of elastic waves from two-point strain measurement.
5. N. Yanagihara 1978 *Bulletin of the Japan Society of Mechanical Engineers* **21**, 1085–1088. New measuring method of impact force.
6. L. Lagerkvist and B. Lundberg 1982 *Journal of Sound and Vibration* **80**, 389–399. Mechanical impedance gauge based on measurement of strains on a vibrating rod.
7. L. Lagerkvist and K. G. Sundin 1982 *Journal of Sound and Vibration* **85**, 473–481. Experimental determination of mechanical impedance through strain measurement on a conical rod.
8. K. G. Sundin 1985 *Journal of Sound and Vibration* **102**, 259–268. Performance test of a mechanical impedance gauge based on strain measurement on a rod.
9. L. G. Karlsson, B. Lundberg and K. G. Sundin 1989 *International Journal of Rock Mechanics Mining Sciences and Geomechanical Abstracts* **26**, 45–50. Experimental study of a percussive process for rock fragmentation.
10. B. Lundberg, J. Carlsson and K. G. Sundin 1990 *Journal of Sound and Vibration* **137**, 483–493. Analysis of elastic waves in non-uniform rods from two-point strain measurement.
11. J. Carlsson, K. G. Sundin and B. Lundberg 1990 *International Journal of Rock Mechanics Mining Sciences and Geomechanical Abstracts* **27**, 553–558. A method for determination of in-hole dynamic force-penetration data from two-point strain measurement on a percussive drill rod.
12. C. Bacon, J. Carlsson and J. L. Lataillade 1991 *Journal de Physique III* (*Suppl., Colloque C*3) **1**, 395–402. Evaluation of force and particle velocity at the heated end of a rod subjected to impact loading.
13. C. Bacon, J. Färm and J. L. Lataillade 1994 *Experimental Mechanics* **34**, 217–223. Dynamic fracture toughness determined from load-point displacement on a three-point bend specimen using a modified Hopkinson pressure bar.
14. C. Bacon 1998 *Experimental Mechanics* **38**, 242–249. An experimental method for considering dispersion and attenuation in a viscoelastic Hopkinson bar.
15. C. Bacon 1999 *International Journal of Impact Engineering* **22**, 55–69. Separation of waves propagating in an elastic or viscoelastic Hopkinson pressure bar with three-dimensional effects.
16. K. G. Sundin and B. O. Åhrström 1999 *Journal of Sound and Vibration* **222**, 669–677. Method for investigation of frictional properties at impact loading.
17. T. Söderström 1994 *Discrete stochastic systems. Estimation and control*. Cambridge: Prentice Hall International (UK) Limited.
18. L. Hillström, M. Mossberg and B. Lundberg 2000 *Journal of Sound and Vibration* **230**, 689–707. Identification of complex modulus from measured strains on an axially impacted bar using least squares.
19. V. Kolousek 1943 *Der Stahlbau* **16**, 5–6 and 11–13. Berechnung der schwingenden Stockwerkrahmen nach der Deformationsmethode.
20. B. Åkesson 1976 *International Journal for Numerical Methods in Engineering* **10**, 1221–1231. PFVIBAT—A computer program for plane frame vibration analysis by an exact method.